A SPECTRAL VOLUME INTEGRAL METHOD USING GEOMETRICALLY CONFORMING NORMAL-VECTOR FIELDS

Teis J. Coenen* and **Martijn C. van Beurden**

Faculty of Electrical Engineering, Eindhoven University of Technology, Den Dolech 2, 5612 AZ Eindhoven, The Netherlands

Abstract—Scattering characteristics of periodic dielectric gratings can be accurately and efficiently computed via a spectral volume integral equation combined with normal-vector fields defined on the grating geometry. We study the impact of the geometrical discretization on the convergence rate of the scattering characteristics for two-dimensional gratings in both TE and TM polarization and compare these with an independent semi-analytical reference for circular cylinders. We demonstrate that geometrically conforming normal vector fields lead to substantially faster convergence and shorter computation times, as opposed to the commonly applied staircasing or slicing.

1. INTRODUCTION

The analysis of electromagnetic scattering by periodic media has received considerable attention for over a century. The study of periodic structures offers the potential to efficiently model the behavior of large repetitive systems that are nowadays encountered in many applications, e.g., semiconductor production, grating couplers, frequency-selective surfaces or phased-array antennas. For a numerical method that incorporates periodicity, it comes natural to use expansions based on Fourier series along the periodic direction(s). Around 1980 the field of grating analysis witnessed a number of new rigorous numerical methods emerging, such as the differential method (DM) [1], the rigorous coupled-wave analysis (RCWA) or Fourier modal method [2, 3], and the C-method [4], which are still widely used

* Corresponding author: Teis J. Coenen (t.j.coenen@tue.nl).

today. The latter two methods address the aperiodic dependence of the solution by either assuming a piecewise constant permittivity, the staircase approximation (RCWA), or by a coordinate transformation of the permittivity profile for each material layer (C-method). The first method (DM) does not remove the aperiodic dependence, but includes the permittivity profile function in its formulation to setup a boundary-value problem that can be solved using a numerical integration technique. The introduction of the Fourier factorization rules [5] greatly improved the convergence, efficiency and accuracy of DM and RCWA, while also the S-matrix method (DM) and the enhanced transmittance approach (RCWA) [2] improved the performance. In the case of DM, the implementation of the Fourier factorization rules [6] was obtained through the introduction of a normal-vector field inside the unit cells, such that the appropriate factorization rules could be applied to the normal and tangential field components separately. This same technique was then applied to the footprint of 2D-periodic gratings in RCWA [7] and made the staircase approximation in the periodic directions superfluous. Nevertheless, the staircase approximation in the aperiodic direction, which is inherent to RCWA, can still introduce scattering that is not present in the smooth structure that is approximated [6]. A perturbative technique based on tilted normal-vector fields has been proposed [8] that can mitigate the scattering from the staircase edges. Although the normal-vector field is not strictly geometrically conformal, it induces a faster convergence.

A comparison of DM, RCWA, and the C-method shows that each method is more efficient for particular grating geometries, such as steep or binary gratings (RCWA), smooth and shallow gratings (DM) or smooth gratings without inclusions (C-method). Moreover, the scaling of computation time and memory requirement with the number of unknowns, which is especially relevant for 2D-periodic gratings, is poor for eigenvalue and boundary-value problems. Therefore, the use of a formulation based on a volume integral equation (VIE) has recently gained interest. Although this formulation in terms of volume will typically lead to a large linear system, it can often be solved efficiently when it is appropriately formulated [9–13]. The combination of VIEs and the introduction of normal-vector fields in the periodic directions results in a similar convergence as compared to RCWA [13] for binary gratings. Contrary to RCWA, the VIE formulation allows for geometrically conforming normal-vector fields with components in both the periodic and the aperiodic direction and provides the opportunity to also remove the staircase approximation in the aperiodic direction. In this work, we introduce geometrically conforming normal-vector fields with components in the aperiodic

direction in a VIE formulation. For testing, a numerical algorithm
has been implemented within the framework of the VIE formulation
described in [11, 13]. To study the effects of geometrically conforming
normal-vector fields, we consider a case of 1D-periodic cylindrical rods,
as it is considered one of the most difficult cases to compute [14]
and an independent reference solution is available. However, the
algorithm can handle gratings with arbitrary height profiles, similar
to [8, 14]. The 1D-periodic case enables us to study the behavior
of the algorithm for a very large number of unknowns per direction
with acceptable computation time and memory demand. We compare
our results with an independent semi-analytical reference solution and
demonstrate that geometrically conforming normal-vector fields lead
to substantially faster convergence and shorter computation times,
as opposed to the staircase-based approach. An example of a recent
application for which a periodic array of cylindrical rods can be used
is the absorption modeling of arrays of nanowires in photovoltaic
applications [15].

2. METHOD OF ANALYSIS

For the numerical tests we consider a low-contrast and a high-contrast
case. The configuration depicted in Fig. 1 is used for either case and
only the permittivity of the cylinder with respect to the background
differs: in the low-contrast case $\varepsilon_r = 2.32$ and in the high-contrast
case $\varepsilon_r = 18.4 - j0.403$, which corresponds to silicon at a wavelength
$\lambda_0 = 500\,\text{nm}$. Note that we assume $\exp(j\omega t)$ time dependence.
The structure is periodic along the x-direction with a period of one
wavelength and is invariant along the y-direction. A plane wave,
with either TE or TM polarization, is incident on the structure with
arbitrary angle $\theta_i = 13°$ with respect to the z-axis. In this situation
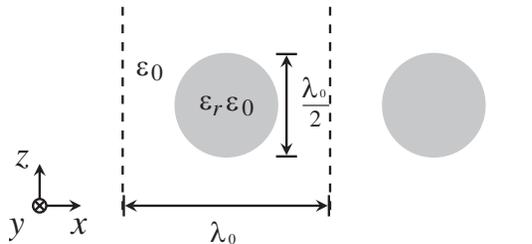
Figure 1. Two unit cells of the 1D-periodic array of infinitely-
extended cylinders considered for the numerical results. λ_0 is the
wavelength in the background medium.

two diffracted components can be distinguished in the reflection: the specular component (zeroth order) and the first order component.

2.1. Reference Solution

For comparison of our results, we have implemented a semi-analytic reference solution. This approach is based on Helmholtz's equation in cylindrical coordinates, for which the solution is expressed in terms of Bessel and Hankel functions in the radial direction and a Fourier expansion in the angular direction. With the use of Graf's addition theorem, the field expansion for a cylinder can be expressed in the local cylindrical coordinates of another cylinder, as is described in more detail in e.g., [17]. In this way, the coupling between the cylinders can be accounted for and an infinite array formulation can be derived. The resulting expression is a double infinite series, with summations over the cylinder index and the cylindrical expansion index. For numerical evaluation the series are truncated. While truncation for the radial expansion index exhibits rapid convergence (relative error below 10^{-11} for a truncation order of 9), the convergence is poor with respect to the number of considered cylinders. Therefore, Aitken's δ^2 process [18, p. 18] is employed to accelerate this convergence. The plot in Fig. 2 shows that the decay in the error is improved considerably by the series acceleration method. In the calculation of the high and
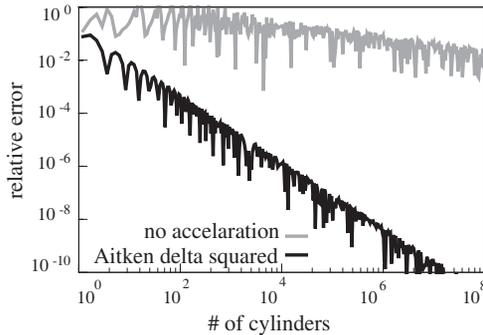
Figure 2. Relative error in the diffraction efficiency as a function of the number of cylinders considered in the truncated sum over the cylinder index in the reference solution. Comparison of the results with and without series convergence acceleration. The reference was calculated by considering $2 \cdot 10^5$ cylinders, truncation order 9 for the number of cylindrical expansion terms and by using convergence acceleration.

low contrast reference solutions we consider $3 \cdot 10^4$ cylinders and a truncation order 9 for the cylindrical expansions such that the relative error of the calculated reference values is less than 10^{-9}.

2.2. Spectral Volume Integral Equation

Below we briefly outline the key ingredients of the spectral VIE formulation for the TE and TM case. For a full description of the employed VIE formulation we refer to [11, 13]. For the TE case, the corresponding matrix equation is given by

$$\left(I + G^{TE} \chi \right) E_y = E_y^i, \tag{1}$$

where I is the identity matrix, G^{TE} is a block-diagonal matrix that represents the Green's function for the TE case, and χ is a block Toeplitz matrix that represents the contrast function in the spectral domain. For the TM case, the matrix equation is given by

$$\left(C_\varepsilon + G^{TM} [\varepsilon C_\varepsilon - C_\varepsilon] \right) \mathbf{F} = \mathbf{E}^i, \tag{2}$$

where C_ε and $\varepsilon C_\varepsilon$ are block Toeplitz matrices that represent field-material interactions with respect to the contrast, and G^{TM} is a block-diagonal matrix that represents the Green's function for the TM case. The field $\mathbf{F}$ is a mix between the electric field $\mathbf{E} = (E_x, E_z)$ and the normalized electric flux density $\hat{\mathbf{D}} = (\hat{D}_x, \hat{D}_z)$, normalized with respect to the permittivity of the background, such that [16]

$$\mathbf{E} = C_\varepsilon \mathbf{F}, \tag{3a}$$

$$\hat{\mathbf{D}} = \varepsilon C_\varepsilon \mathbf{F}, \tag{3b}$$

which means that only a single matrix-vector multiplication is needed to obtain $\mathbf{E}$ or $\hat{\mathbf{D}}$ once $\mathbf{F}$ is available. The field-material operators C_ε and $\varepsilon C_\varepsilon$ contain a so-called normal-vector field that describes the local normal vector on an interface between two dielectric media. In particular, the normal-vector field combines the normal component of $\hat{\mathbf{D}}$ and the tangential component of $\mathbf{E}$ to form the vector $\mathbf{F}$. We note that, following the notation of [16], C_ε and $\varepsilon C_\varepsilon$ represent each a different operator, i.e., $\varepsilon C_\varepsilon$ is not constructed from C_ε.

Owing to the structure of the separate matrices in the above equations, an efficient $\mathcal{O}(N_z M \log M)$ matrix-vector product is obtained, where N_z is the total number of unknowns, i.e., samples, in the aperiodic direction (z) and M is the total number of unknowns, i.e., Fourier modes, in the periodic direction (x). The memory storage requirement is $\mathcal{O}(N_z M)$. Therefore the above matrix equations are solved iteratively using the stabilized-biconjugate-gradient (Bi-CGSTAB(2)) method.

2.3. Geometrical Approximation: Slicing Versus Conformal

In the traditional approach for normal-vector fields with components in the periodic direction only, the cylinder is approximated by a stack of piecewise binary slices. As depicted in Fig. 3(a), the cylinder is divided into sectors with equal arc length to ensure adequate discretization of the cylinder's curvature. The original volume is retained for each slice. In the VIE formulation each slice is discretized in the z-direction. The number of samples per slice $N_{z,\text{slice}}$ is based on the thickness ratio compared to the thinnest slice for which $N_{z,\text{slice}} = 2$. This results in an approximately uniform sampling along the z-axis. We will refer to this traditional approach as slicing. Alternatively, a geometry-conformal approach can be adopted in which the entire geometry is sampled in the aperiodic direction without the intermediate slicing of the geometry. The impact for the TE case is negligible, since only the Fourier transform of the contrast function at each sample point is needed for the matrix χ in Eq. (1). However, for the TM case, the matrices C_ε and $\varepsilon C_\varepsilon$ in Eq. (2) with and without slicing are completely different due to the presence of the normal-vector field. Both matrices can be partitioned as

$$C = \begin{pmatrix} C_{xx} & C_{xz} \\ C_{zx} & C_{zz} \end{pmatrix}, \tag{4}$$

where each of the sub-matrices is a Toeplitz matrix per sample point along z. In the case of slicing, the normal-vector field is purely x directed, which leads to $C_{xz} = C_{zx} = 0$, i.e., the zero matrix, and $C_{\varepsilon,zz}$ equals the identity matrix. Hence this case requires only FFTs for the convolutions in $[\varepsilon C_\varepsilon - C_\varepsilon]_{xx}$, $[\varepsilon C_\varepsilon - C_\varepsilon]_{zz}$ and $C_{\varepsilon,xx}$, which amounts to 2 forward and 3 backward FFTs and 3 diagonal matrix multiplications per sample point in case of slicing. For the TM case without the intermediate slicing, all four submatrices of C_ε and $[\varepsilon C_\varepsilon - C_\varepsilon]$ are full Toeplitz matrices per sample point and no simplification takes place. As a consequence, a total of 2 forward and 4 backward FFTs and 8 diagonal matrix multiplications per sample point are required for the field-material interactions. Additionally, a geometrically conformal normal-vector field must be determined. For the TM case, this comparison shows that the slicing approach is both very flexible and computationally more efficient than the geometrically conformal approach for the same number of unknowns, especially since the FFTs constitute the main computational burden. Consequently, the geometrically conformal approach will outperform the slicing approach when a predefined accuracy level is obtained with fewer unknowns as compared to the number of unknowns required for the same accuracy with the slicing approach.
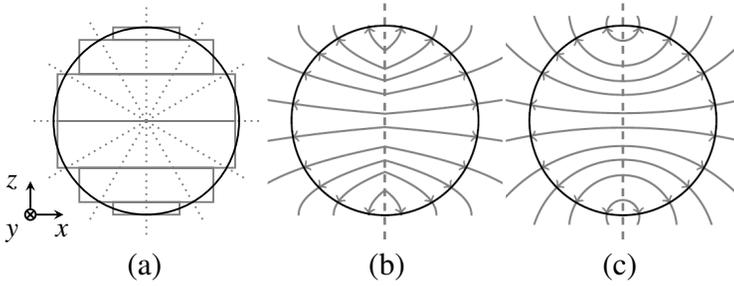
Figure 3. Applied slicing strategy using a staircase approximation and the two utilized types of normal-vector fields NVA and NVB. At the boundaries the normal vector points outward and the direction flips at the dashed line. (a) Slicing. (b) NVA. (c) NVB.

Since normal-vector fields are not uniquely defined, an adequate implementation has to be chosen for our geometry. For a cylinder with the restriction of outward-pointing normal vectors, the simplest implementation is a vector field with a tilt angle that is dependent on z only. The tilt is chosen such that the field is normal to the cylinder boundary at each z-coordinate and that its x-component changes sign at the dashed line as depicted in Fig. 3(b). We note that there is a kink in the field lines, due to the non-zero z-components at the dashed line. In the following we will refer to this normal-vector field as implementation NVA.

An alternative, that exhibits smoother convergence, is based on a normal-vector field with circular field lines, as depicted in Fig. 3(c). The circles are orthogonal to the cylinder boundaries and the dashed line in the plot. The x-component of the normal-vector field changes sign at the dashed line where also its z-component vanishes. We will refer to this implementation as NVB. Because of the smoother convergence, implementation NVB is preferred over NVA and we will we use NVB for our calculations, unless explicitly specified otherwise.

3. NUMERICAL RESULTS

We investigate the convergence behavior as a function of the discretization in the periodic and aperiodic directions and the computation time.

3.1. Convergence in the Periodic Direction

First, we relate our approach to DM, based on the results presented in [14, Fig. 8], by comparing the convergence of the error in the case of

TM polarization with respect to the truncation order M, which is the upper index of the Fourier modes and corresponds to a total of $2M+1$ Fourier modes in the periodic direction. The analyzed geometry is a dielectric cylindrical rod grating with a period of $1.58\lambda_0$ and cylinders with $0.79\lambda_0$ diameter and $\varepsilon_r = 6.25$. The results in [14] have been obtained using in total 400 integration points in the aperiodic direction. A TM polarized plane wave with angle $\theta_i = 30°$ with respect to the z-axis is incident on the grating. We have generated a reference solution with $3 \cdot 10^4$ cylinders and truncation order 17 for the cylindrical expansions. In Fig. 4 the results from [14] have been plotted, as well as the results that have been obtained with the volume integral method. The error plotted in Fig. 4 follows the definition in [14]. We observe that the convergence trends for both methods are similar for the case with slicing. If we compare the approaches based on geometrically conforming normal-vector fields, we observe that the convergence of NVA exhibits an oscillatory effect, but overall it converges at a similar rate as DM. NVB also converges at the same rate, but the error is a factor 10 to 100 lower at equal truncation orders. Below 10^{-6} the convergence rate of NVA and NVB with $N_z = 400$ reduces. This effect also appears to be present in the results for DM and is caused by the discretization in the aperiodic direction: the convergence of the error for NVB with $N_z = 5960$ is not hampered by this effect.

For our further study of the convergence in the periodic direction, we go back to the scattering setup described at the beginning
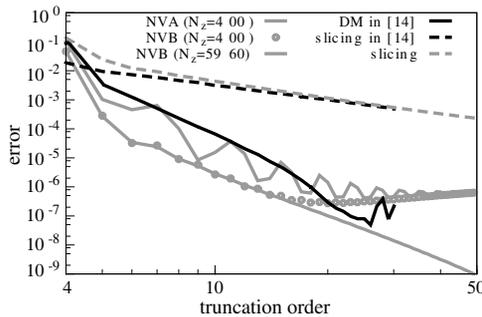
Figure 4. Error in TM polarization as a function of the truncation order for the cylindrical rod grating presented in [14, Fig. 8]. The definition of the error is according to [14]. Comparison of the volume integral method (gray) with DM (black). Comparison for NVA and NVB types of normal-vector fields. For the cases without slicing $N_z = 400$ or $N_z = 5960$ and in the case of slicing $N_s = 100$ with 4 unknowns per slice.

of Section 2 and we choose a fixed and very fine discretization in the z-direction with $N_z = 5960$ sample points. In the case of slicing, the sample points are distributed (approximately) uniformly over 120 binary slices and in the geometrically exact implementations the samples are distributed uniformly.
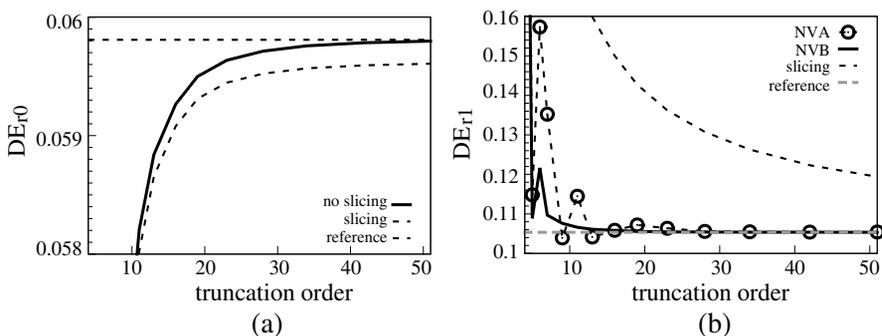
Figure 5. Diffraction efficiency of the reflected orders as a function of the truncated number of Fourier modes for a high-contrast grating with $N_z = 5960$. Comparison of slicing and two different normal-vector field implementations (NVA and NVB) with a reference solution. (a) TE polarization; specular component. (b) TM polarization; first order component.

First we consider the diffraction efficiency (DE) [19, Ch. 2] of the reflected components as a function of the truncation order M. In Fig. 5(a) the diffraction efficiencies for the specular reflection in TE polarization are depicted for the high-contrast cylinders. The dashed gray line indicates the diffraction efficiency that has been calculated using the semi-analytical reference method. The curve representing the method without slicing converges to the reference solution. The results obtained with slicing converge to a slightly different diffraction efficiency. Since the slicing, and therefore the geometry, is fixed, the difference is due to the geometrical discrepancy between the sliced and the sampled smooth structure, since TE polarization does not require normal-vector fields. A finer slicing is required to obtain more accurate values.

Figure 5(b) depicts the diffraction efficiency for the first order reflection in TM polarization. For this polarization, normal-vector fields are used to distinguish between normal and tangential field components and depending on the normal-vector field choice we observe different results. For NVA the convergence shows an oscillatory

convergence behavior, whereas for NVB the convergence is smoother. Furthermore, it is evident that the convergence with slicing is considerably slower than the normal-vector based methods.

Additionally, we investigate the behavior of the relative error with respect to the reference solution of the total diffraction efficiency, i.e., $DE_{r0} + DE_{r1}$," for the two reflected orders, defined by

$$\frac{|(DE_{r0} + DE_{r1}) - (DE_{r0}^{ref} + DE_{r1}^{ref})|}{(DE_{r0}^{ref} + DE_{r1}^{ref})}. \tag{5}$$

Note that this error definition is not squared as in [14] and Fig. 4. In Fig. 6 this relative error has been plotted for the two considered contrasts and polarizations for both the normal-vector methods and the slicing method.
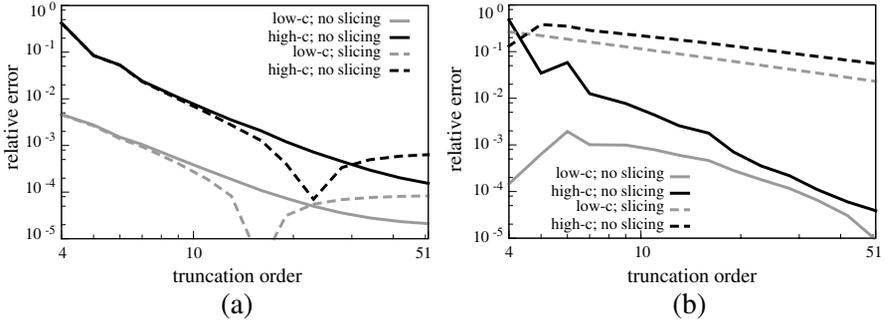
Figure 6. Relative error in the total reflection diffraction efficiency of the reflected orders as a function of the truncated number of Fourier modes for a low-contrast (gray) and a high-contrast (black) grating with $N_z = 5960$. Solid lines: no slicing and NVB; dashed lines: slicing based on 120 slices). (a) TE polarization. (b) TM polarization.

For incident waves with TE polarization, see Fig. 6(a), we observe that the difference between the high- and low-contrast cases manifests itself in a scaling factor in the relative error. Comparing the methods with and without slicing, we see that for low truncation orders the curves coincide. When more Fourier modes are considered, the convergence rate appears to decrease and it seems that the relative error is bounded by a minimum value, which is smaller when no slicing is applied. In the case of slicing, the geometrical discrepancy limits the accuracy, while in the other case the number of samples in the z-direction limits the accuracy. To further improve the accuracy, the number of aperiodic unknowns needs to be increased further.

The relative error in the case of TM polarization as shown in Fig. 6(b) exhibits a different behavior, due to the normal-vector field. While the high- and low-contrast cases for slicing seem to differ again by a scaling factor, the error trends for NVB and slicing converge at different rates, where the former converges much faster. The poor convergence for the slicing method for TM polarization is due to the staircase approximation, which introduces strong near fields at the square slice edges [6]. Since the normal-vector field method accounts for the slope of the object boundaries, the unwanted near-field fluctuations are not introduced and therefore it does not suffer from such considerable convergence deterioration for TM polarization.

3.2. Convergence in the Aperiodic Direction

The convergence for unknowns in the z-direction is treated in a similar way as in the periodic direction, by fixing the truncation order and varying the number of slices or the number of sample points directly (geometrically conforming normal-vector case). The relative defined in (5) has been plotted in Fig. 7 for the same situations as in Fig. 6, using a total of 103 Fourier modes.
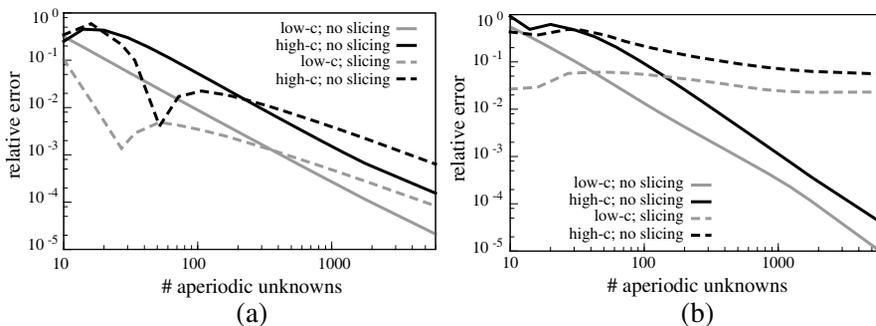
Figure 7. Relative error in the total reflection diffraction efficiency of the reflected orders as a function of the unknowns in the z-direction N_z for a low-contrast (gray) and a high-contrast (black) grating with $M = 51$. Solid lines: no slicing and NVB; dashed lines: slicing. (a) TE polarization. (b) TM polarization.

For the case of TE polarization, depicted in Fig. 7(a), the low- and high-contrast cases differ again in relative error by a scaling factor. The convergence tends to constant rates, contrary to the convergence with respect to Fourier truncation where the error appeared to be bounded.

Due to the staircase approximation, the convergence rate with slicing is worse than when the geometry is not approximated.

The convergence trends for the aperiodic unknowns in the case of TM polarized waves, plotted in Fig. 7(b), are roughly comparable to those in Fig. 6(b) for Fourier truncation order dependence. In the TM polarized cases NVB improves the convergence order of the relative error considerably.

3.3. Trends for Computation Time

Apart from the convergence with respect to the number of unknowns, for many applications it is also relevant to study the relation between accuracy and computation time. For this, both the truncation order and the number of unknowns in the z-direction are varied simultaneously and the relative errors in the diffraction efficiencies of the reflected orders have been calculated for all combinations of unknowns as given in Table 1. All computations have been performed on a HP EliteBook 8530w with an Intel Core2 Duo T9600 2.80 GHz CPU and 3 GB of accessible memory. To facilitate the comparison of the results for different grating contrast and polarization, the computation times have been normalized to the maximum computation times per plot, which are specified in the captions of Fig. 8 and Fig. 9.

In Fig. 8 the relative error for TM polarization has been plotted as a function of the computation time for each variation. On a double
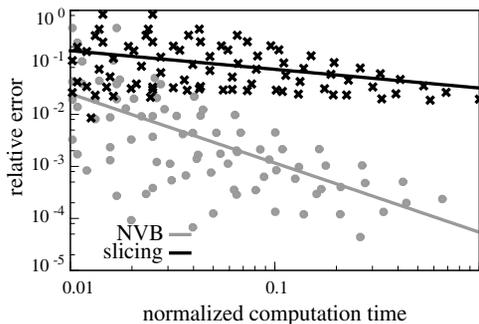
Figure 8. Relative error as a function of the computation time, normalized to 16.6 s, for different combinations of truncation order and unknowns in the z-direction. The linear trends are the least-squares fit to the scattered data. Results comparing a geometrically conformal and a sliced grating with low contrast and TM polarization.
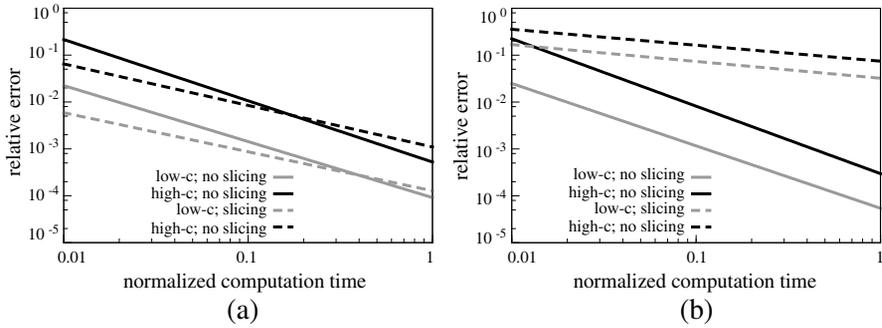
Figure 9. Least-squares fit of the relative error in the total diffraction efficiency of the reflected orders as a function of the normalized computation time. Based on simultaneous variation of truncation order and unknowns in the z-direction for a low-contrast (gray) and a high-contrast (black) grating. Solid lines: no slicing and NVB; dashed lines: slicing. The normalization unit corresponds to 12.0 s, 82.3 s, 16.6 s, and 718 s for TE low- and high-contrast and TM low- and high-contrast, respectively. (a) TE polarization. (b) TM polarization.

logarithmic scale we discern that the data points are approximately scattered around a straight line. By performing a least-squares fit to the scattered data, we obtain the trend lines in Fig. 8. We note that the best performance is achieved at the lower envelope of the scattered data, however a priori determination of the optimal number of unknowns in all directions simultaneously is intractable. Therefore, the linear trends are more indicative of the convergence rates of the relative errors as a function of computation time. The fitted linear trends have been plotted for the case of TE and TM polarization in Fig. 9(a) and Fig. 9(b), respectively. Note that the trends of Fig. 8 are represented by the gray lines in Fig. 9(b). For TE incidence we observe that the trends for the low- and high-contrast gratings differ by an offset in the relative error. Furthermore, the computation time for low accuracy is lower in the case of slicing. However, since the trends for the cases without slicing decrease at a higher rate, the latter approach is preferable for higher accuracies ($< 10^{-3}$ for the low contrast and $< 10^{-2}$ for the high contrast).

In the case of TM polarization, an offset in the relative error is also present between the high- and low-contrast cases. The decay rate for NVB is approximately equal to the rate for TE polarization. However, the slicing method clearly exhibits a much lower convergence rate. The normal-vector field method is faster than slicing for all accuracies.

Table 1. Settings for the number of unknowns that have been used for the presented computations. The discretezation is approximately equidistant on a logarithmic scale.

Method	Fourier trunc. order (M)	Aperiodic unknowns (N_z)
slicing	$\{1, 2, 3, 4, 5, 6, 8, 11, 14, 18,$ $23, 30, 39, 51\}$	$\{2, 4, 7, 10, 22, 27, 52, 81, 136,$ $238, 421, 719, 1236, 2174\}$
no slicing	$\{1, 2, 3, 4, 5, 6, 8, 11, 14, 18,$ $23, 30, 39, 51\}$	$\{2, 3, 4, 6, 10, 16, 26, 41, 65, 103,$ $164, 261, 415, 660, 1049\}$

4. CONCLUSION

We have introduced geometrically conforming normal vectors within a volume integral equation formulation for 1D-periodic gratings, to improve the computational performance and such that the method can be applied to gratings with arbitrary height profiles. For cylindrical gratings of low and high dielectric contrast, we have investigated the performance of this approach and we have compared the accuracy to an independent reference solution.

Studying the convergence of the diffraction efficiencies with respect to the number of Fourier modes, we have observed that the accuracy of the traditional staircase approximation is limited by the geometrical discrepancy between the approximated cylinder and the true cylinder.

For TM polarization we have also observed that the convergence rate of the geometrically conforming normal-vector approach is higher for both high- and low-contrast gratings, which is consistent with improvements obtained for the differential method. We have observed similar trends for the convergence with respect to the aperiodic discretization. Moreover, the convergence rate with respect to the aperiodic discretization is also slightly higher for TE polarization when slicing is not applied.

We have observed that only for low accuracies and TE polarization the slicing method is faster than the geometrically exact approach. For all other cases the convergence rate with respect to computation time is higher for the geometrically conforming normal-vector approach than for the approach based on slicing.

REFERENCES

1. Neviere, M., R. Petit, and M. Cadilhac, "About the theory of optical grating coupler-waveguide systems," *Optics Communications*, Vol. 8, No. 2, 113–117, 1973.

2. Moharam, M. G. and T. K. Gaylord, "Rigorous coupled-wave analysis of planar-grating diffraction," *Journal of the Optical Society of America*, Vol. 71, No. 7, 811–818, 1981.

3. Botten, L. C., M. S. Craig, R. C. McPhedran, J. L. Adams, and J. R. Andrewartha, "The dielectric lamellar diffraction grating," *Opt. Acta*, Vol. 28, 413–428, 1981.

4. Chandezon, J., G. Raoult, and D. Maystre, "A new theoretical method for diffraction gratings and its numerical application," *J. of Optics*, Vol. 11, No. 4, 235–240, 1980.

5. Li, L., "Use of Fourier series in the analysis of discontinuous periodic structures," *Journal of the Optical Society of America A*, Vol. 13, No. 9, 1870–1876, 1996.

6. Popov, E., M. Nevière, B. Gralak, and G. Tayeb, "Staircase approximation validity for arbitrary-shaped gratings," *Journal of the Optical Society of America A*, Vol. 19, No. 1, 33–42, 2002.

7. Schuster, T., J. Ruoff, N. Kerwien, S. Rafler, and W. Osten, "Normal vector method for convergence improvement using the RCWA for crossed gratings," *Journal of the Optical Society of America A*, Vol. 24, No. 9, 2880–2890, 2007.

8. Rafler, S., P. Götz, M. Petschow, T. Schuster, K. Frenner, and W. Osten, "Investigation of methods to set up the normal vector field for the differential method," *Proc. SPIE*, Vol. 6995, 9, 2008.

9. Magath, T. and A. Serebryannikov, "Fast iterative, coupled-integral-equation technique for inhomogeneous profiled and periodic slabs," *Journal of the Optical Society of America A*, Vol. 22, No. 11, 2405–2418, 2005.

10. Magath, T., "Coupled integral equations for diffraction by profiled, anisotropic, periodic structures," *IEEE Transactions on Antennas and Propagation*, Vol. 54, 681–686, 2006.

11. van Beurden, M. C., "Fast convergence with spectral volume integral equation for crossed block-shaped gratings with improved material interface conditions," *Journal of the Optical Society of America A*, Vol. 28, No. 11, 2269–2278, 2011.

12. Shcherbakov, A. A. and A. V. Tishchenko, "New fast and memory-sparing method for rigorous electromagnetic analysis of 2D periodic dielectric structures," *Journal of Quantitative Spectroscopy and Radiative Transfer*, Vol. 113, 158–171, 2012.

13. van Beurden, M. C., "A spectral volume integral equation method for arbitrary bi-periodic gratings with explicit Fourier factorization," *Progress In Electromagnetics Research B*, Vol. 36, 133–149, 2012.

14. Popov, E. and M. Nevière, "Grating theory: New equations in Fourier space leading to fast converging results for TM polarization," *Journal of the Optical Society of America A*, Vol. 17, No. 10, 1773–1784, 2000.

15. Sturmberg, B. C. P., K. B. Dossou, L. C. Botten, A. A. Asatryan, C. G. Poulton, C. M. de Sterke, and R. C. McPhedran, "Modal analysis of enhanced absorption in silicon nanowire arrays," *Optics Express*, Vol. 19, No. S5, A1067–A1081, 2011.

16. Popov, E. and M. Nevière, "Maxwell equations in Fourier space: Fast-converging formulation for diffraction by arbitrary shaped, periodic, anisotropic media," *Journal of the Optical Society of America A*, Vol. 18, No. 11, 2886–2894, 2001.

17. Elsherbeni, A. Z. and A. A. Kishk, "Modeling of cylindrical objects by circular dielectric and conducting cylinders," *IEEE Transactions on Antennas and Propagation*, Vol. 40, No. 1, 96–99, 1992.

18. Abramowitz, M. and I. Stegun, *Handbook of Mathematical Functions with Formulas, Graphs, and Mathematical Tables*, Dover Publishing, New York, 1972.

19. Popov, E., Editor, *Gratings: Theory and Numeric Applications*, Institut Fresnel, CNRS, AMU, 2012, www.fresnel.fr/numerical-grating-book.